12.7 Wave Spectrum Data

The energy spectrum of the dynamic air-water surface is a powerful modern analytical tool which may be used to describe the intricate geometric and physical features of the air-water surface. In particular, our study of the energy spectrum in Sec. 12.4 showed how it may be used as a source of information on the mean square slopes and heights of the air-water surface, quantitites which, as will be shown in Sec. 12.11, are of importance in the description of radiative transfer phenomena at the surface. In this section we shall review some current means of obtaining experimental data on wave energy spectra of the dynamic air-water surface. We shall review three such procedures based on three fundamentally different principles.

The first procedure to be described uses aerial stereo photographs of the sea surface taken from flying aircraft; the second records the motions of small floating buoys with sensitive positional and orientational recorders inside; the third uses sonic echo transducers directed upward toward the waves from the deck of a hovering submerged submarine. Each of these three procedures has one principal goal: the determination of the one-dimensional spectrum T_k (or its equivalents T_σ, T_τ) as defined in (102) of Sec. 12.4, or hopefully, with enough probes and resolution, the full two-dimensional spectrum $E(\mathbf{k})$ (or its equivalents S, F) as defined in (75) of Sec. 12.4. In regard to the matter of resolution, radiative transferists perusing the following exposition will observe that in each case the resolution does not quite extend into the capillary region of the wave spectra. This region is of particular importance to optical calculations. However, each method is capable in principle of having its resolution increased, and it is for this reason that the reviews are presented in some detail, to supplement the descriptions of the electrical and optical methods of Duntley, and Cox and Munk given in Sec. 12.5.

Wave Spectra by Aerial Stereo Photography

Imagine that the dynamic air-water surface may be instantaneously frozen in its motion and suppose that a survey team is dispatched to make a contour map of the surface much in the manner that a contour map of hilly and mountainous country is made by survey parties with theodolites and level rods. Such a contour map of the frozen air-water surface along with the main analytical relations of harmonic analysis developed in Sec. 12.4, may be used to construct a detailed picture of the unresolved energy spectrum $\overline{E}(\mathbf{k},t)$ of the surface, as defined in (61) of Sec. 12.4. This seemingly miraculous event of freezing the water surface was in effect accomplished (optically) in November of 1954 when two camera-laden airplanes flew over a certain stretch of the North Atlantic Ocean and, as schematically depicted in Fig. 12.41, took a set of simultaneous pairs of photographs of that region of ocean. Each pair of photos allowed the same patch of surface to be viewed from two different vantage points, thereby producing a set of stereo photographic pairs of the region; that is, photographs were obtained which, when viewed

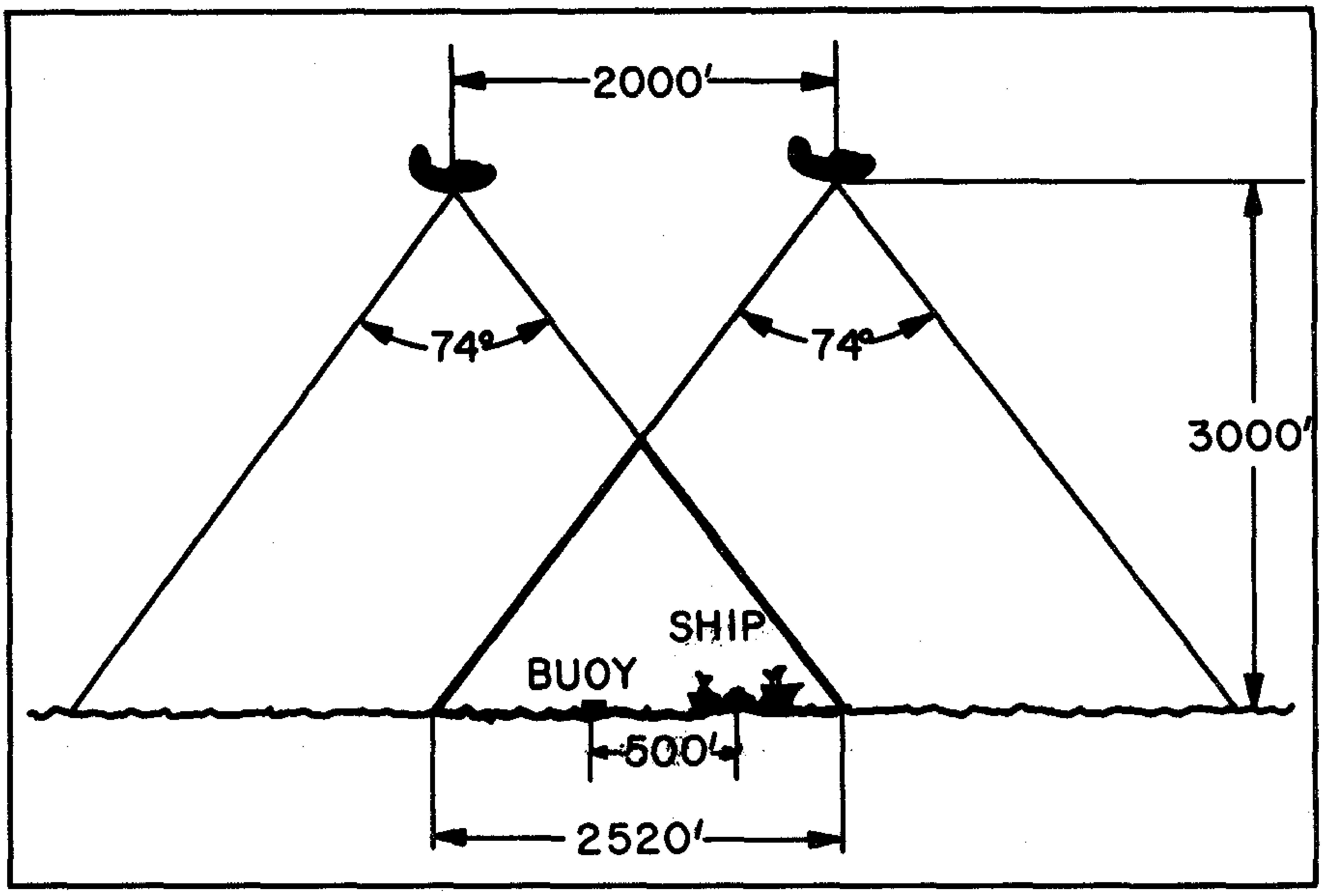

FIG. 12.41 Schematic arrangements of the Stereo Wave Observation Project aircraft carrying the synchronized cameras. Their common field of view is shown. Stereo photographs of the air-water surface in the common field were the basis of an extensive computation program leading to a spectrum of the observed sea surface.

through special optical equipment, would permit the hills and hollows of the dynamic surface to be directly perceived and measured. Within view of both cameras was the Woods Hole research vessel, *Atlantis*, and also a floating buoy. The *Atlantis* and the buoy were to help provide a photogrammatic basis for the processing of the stereo pairs and the buoy, in addition, was recording the motion of the sea directly via its own response to the passing waves.

Months of preparation went into that flight in November 1954 to provide in a matter of seconds, a detailed stereo photographic record of nearly five million square feet of ocean surface; months of work were yet ahead to numerically process the data to obtain the desired results. This mammoth project was designated as the *Stereo Wave Observation Project* ("SWOP"), and was carried out under the auspices of the New York University College of Engineering Research Division, by the departments of Meteorology, Oceanography, and the Engineering Statistics Group, and with the help of various local naval installations and the Woods Hole Oceanographic Institution. A full report of the history of the project, its conception, development, and its results are contained in [45], [52]. Our main purpose here is to review only a few of the manifold results of the project, namely those that touch on the computed form of the two-dimensional energy spectrum $F(\sigma,\phi)$, the one-dimensional spectrum T_σ, and the wave-slope wind-speed law.

To prepare the photographs for numerical processing, each photo of the best pairs of photos was reduced to 5400 numbers on a rectangular grid. The wave pole (the floating buoy) records were converted to a discrete time series of about 1800 numbers each. The purpose of the wave pole records was to provide an independent check on the information derived from the 10,800 stereo grid points. The guiding principle behind the ensuing computations is represented by the formulas:

$$\bar{E}(\mathbf{k}) = \frac{1}{4\pi^2} \int_{E_2} \phi(\mathbf{x},0) \cos (\mathbf{k}\cdot\mathbf{x})\, dV(\mathbf{x}) \qquad (1)$$

$$\bar{E}(\mathbf{k}) = \frac{1}{2} (E(\mathbf{k}) + E(-\mathbf{k})) \qquad (2)$$

$$E(\mathbf{k}) = \frac{1}{2} \mathcal{A}^2(\mathbf{k}) \qquad (3)$$

$$\zeta(x,0) = \int_{E_2} \mathcal{A}(\mathbf{k}) \cos (\mathbf{k}\cdot\mathbf{x})\, dV(\mathbf{k}) \qquad (4)$$

which follow from (61)-(80) of Sec. 12.4 with phase $\varepsilon = 0$. Furthermore the autocorrelation integral over E_2 (cf., (74) of Sec. 12.4) is assumed independent of t, reflecting the assumed stationary nature of the physical processes taking place over the ocean surface at the time of the photographs.

The theoretical procedure used in the SWOP data reduction was first to generate a contour map of the air-water surface under study. A sample contour sheet is shown in Fig. 12.42. The locations of the ship and buoy may be discerned near the center of the map. The contour interval is 3 feet, with vertical distances accurate to two feet (about 0.2 mm on the map), and horizontal distances accurate to 2 feet. Next, the autocorrelation function $\phi(\mathbf{x},0)$ was computed by discretizing the contour map data and using a discrete version of (74) of Sec. 12.4:

$$\phi(\mathbf{x},0) = \lim_{r\to\infty} \frac{1}{\pi r^2} \int_{S_r(0)} \zeta(\mathbf{x}+\mathbf{y},s)\, \bar{\zeta}(\mathbf{y},s)\, dV(\mathbf{y}) \ . \qquad (5)$$

Once $\phi(\mathbf{x},0)$ in (5) was found, the discrete version of (1) was computed to find $\bar{E}(\mathbf{k})$. Equations (2) and (3) show the connection between the unresolved energy spectrum $\bar{E}(\mathbf{k})$, the resolved energy spectrum $E(\mathbf{k})$, and the amplitude spectrum $\mathcal{A}(\mathbf{k})$ of the air-water surface. It is clear from (2) that by means of a single stereo photograph pair, one can find only the average of $E(\mathbf{k})$ and $E(-\mathbf{k})$, unless it is happily found that there is a certain direction, say $\mathbf{k}_0$, such that $E(k') = 0$ for all $\mathbf{k}'$ whenever $\mathbf{k}' \cdot \mathbf{k}_0 < 0$. In other words it may happen that all the waves on the sea are traveling within 90° of a fixed direction $\mathbf{k}_0$, which is usually the mean wind direction in an open sea. If this is the case (and the assumption is

FIG. 12.42 The contour map resulting from the stereo photographs of Fig. 12.41. The ship and buoy are visible near the center of the map.

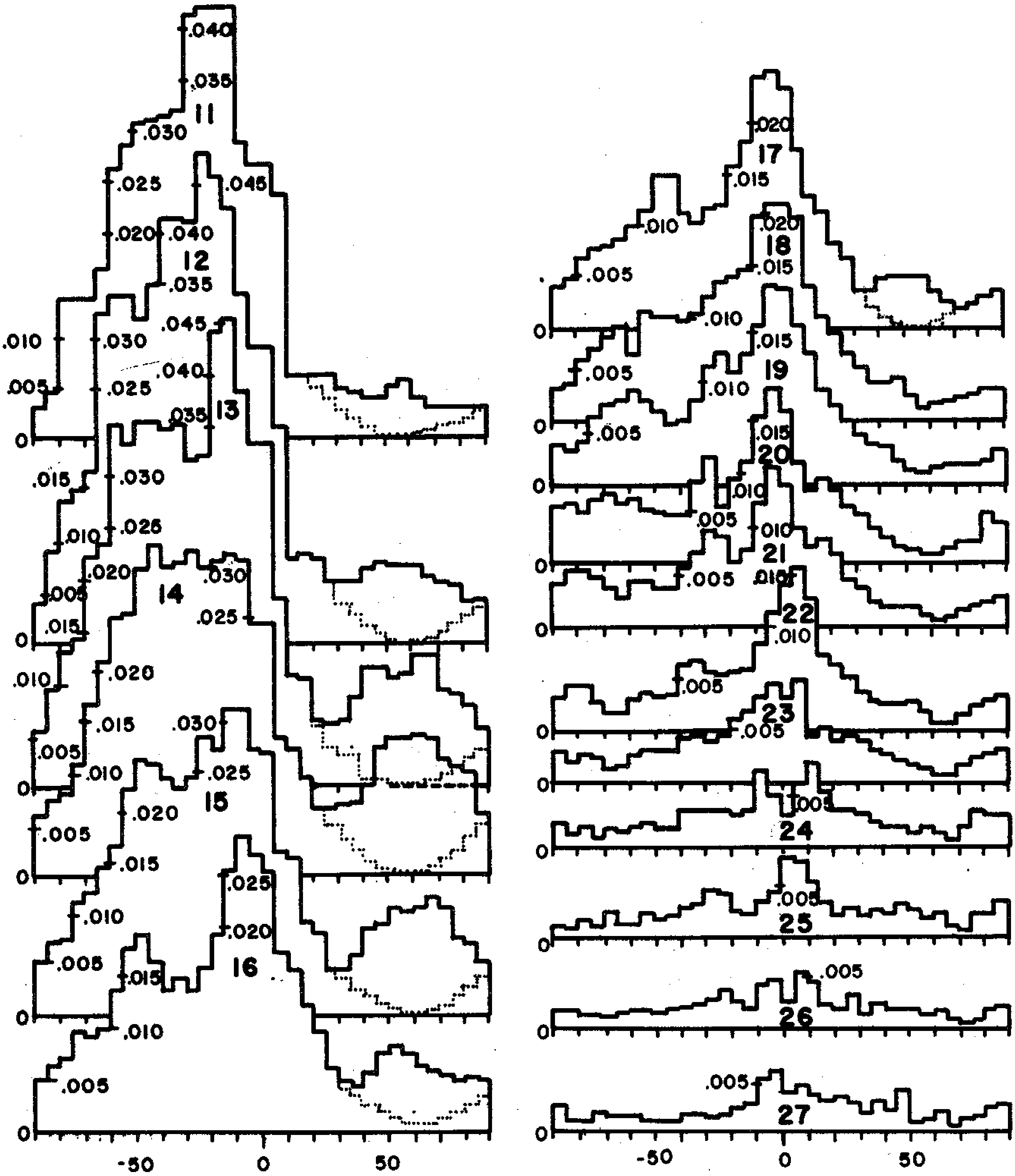

FIG. 12.43 Seventeen histograms of the directional spectrum $F(\sigma,\phi)$ of air-water surface as derived from the data SWOP experiment (Fig. 12.42). Each histogram is a plot of $F(\sigma,\phi)$ as a function of ϕ for a given σ (see text).

occasionally not unreasonable) then $\bar{E}(\mathbf{k}) = E(\mathbf{k})/2$ for all $\mathbf{k}$ whose directions lie within 90° of $\mathbf{k}_o$, and $E(\mathbf{k}) = 0$ elsewhere. This assumption was adopted by the SWOP analysis.

Figure 12.43 shows the computed energy spectrum in the form of histograms, as they emerged from the computations using a discrete version of (1). For computation purposes, the *temporal frequency* form $F(\sigma,\phi)$ of the energy spectrum was adopted (cf. (107) of Sec. 12.4). Hence the ordinates of each histogram in Fig. 12.43 are values of $F(\sigma,\phi)$. The abscissas take values over angles ϕ varying ± 90° from the mean wind direction k_o. Each histogram is distinguished from another by its temporal frequency σ, which took one of seventeen discrete values $\sigma = 2\pi j/96$, $j = 11, 12, \ldots, 26, 27$.

The analysts of the SWOP report were able to obtain, after a considerable amount of subjective curve fitting, an indealized energy spectrum from the preceding data in the form:*

$$F(\sigma,\phi) = \frac{\pi}{4} c_1 \sigma^{-6} e^{-2(g/\sigma U_a)^2} \cdot f(\sigma,\phi) \qquad (6)$$

where we have written:

$$\text{"}f(\sigma,\phi)\text{"} \quad \text{for} \quad \frac{1}{\pi}\left[1 + \left(0.50 + 0.82\, e^{-\frac{1}{2}\left(\frac{\sigma U_a}{g}\right)^4}\right) \cos 2\phi + \left(0.32\, e^{-\frac{1}{2}\left(\frac{\sigma U_a}{g}\right)^4}\right) \cos 4\phi\right] \qquad (7)$$

for ϕ in the range $[-\pi/2, \pi/2]$, and where:

$$c_1 = 3.05 \times 10^4 \text{ cm}^2 \text{ sec}^{-5} \quad .$$

Here U_a is the wind speed in centimeters per second observed during the experiment, namely 18.7 knots at an anemometer height of 15 feet. (All SWOP units are in the c.g.s. system unless noted otherwise.) This determination of (6), especially as regards the two powers of σ and U_a occurring in the equation, is a remarkable feat considering that all this comes from only one stereo pair. As we shall see later this energy spectrum yields a one-dimensional Neumann type of spectrum T_σ obtained by completely different means in different times [189]. Indeed, by integrating (6) over all ϕ (and recalling $F(\sigma,\phi) = 0$ for $|\phi| > 90°$) we have from (110) of Sec. 12.4:

$$T_\sigma = \int_0^{2\pi} F(\sigma,\phi)\, d\phi = \frac{\pi}{4} c_1 \sigma^{-6} e^{-2(g/\sigma U_a)^2} \qquad (8)$$

which is the gestalt of the Neumann spectrum [189] in temporal frequency form (see (8) of Sec. 12.8). In Fig. 12.44 the theoretical Neumann (temporal frequency) spectrum T_σ is compared with the stereo spectrum obtained by integrating the $F(\sigma,\phi)$ in Fig. 12.43 over ϕ for each $\sigma = 2\pi j/96$. The spectrum T_σ was also estimated by means of the bobbing buoy, and this version of T_σ is denoted by "wave pole spectrum" in the figure. The general visual agreement among the three spectra, arising from such diverse means of development, is quite

---

*Readers who will study the SWOP report [45] in conjunction with the present work, should note that our u,v pair with SWOP's α,β, respectively. Furthermore our σ,ϕ pair with μ,θ; our $E(u,v)$ with $A*(\alpha,\beta)]^2/2$; our $F(\sigma,\phi)$ with $[A(\mu,\theta)]^2/2$.

Errata

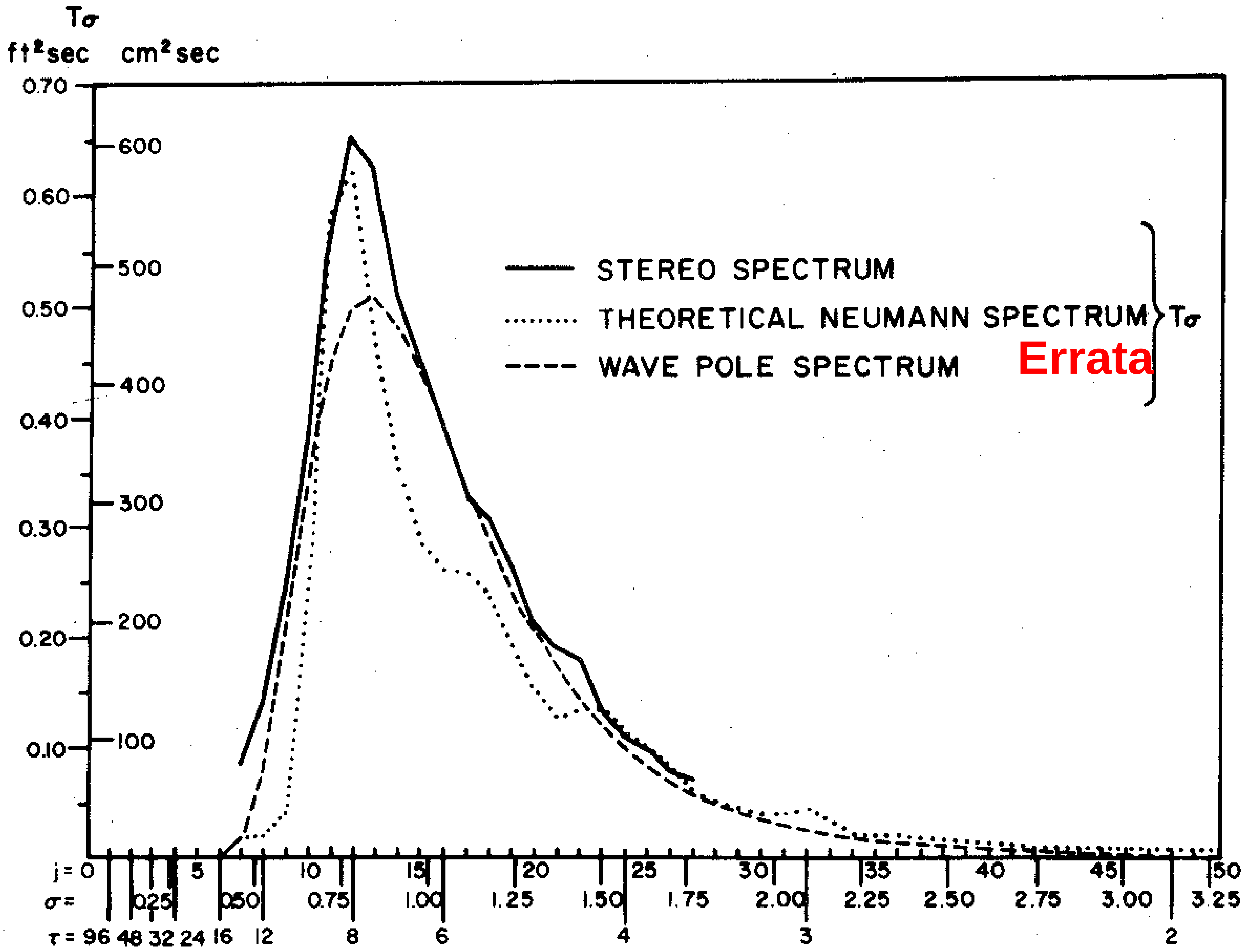

FIG. 12.44 By integrating each histogram in Fig. 12.43 over ϕ, plots of the temporal energy spectrum T_σ could be made and compared with independent estimates of T_σ, as given by Neumann and by the wave pole (buoy) readings of the SWOP experiment.

good. It must be noted, however, that a comparison such as this, based on only one stereo pair, and an *ad hoc* fit at that, is hardly conclusive evidence for the Neumann spectrum. Further study has shown [33] that the Bretschneider spectrum (cf. Sec. 12.9) fits the SWOP data just as well.

As a final matter in the survey of the SWOP results, we cite the version of the wave-slope wind-speed law evolved by the stereo project. It was found that:

$$\sigma_u^2 = 0.99 \times 10^{-3}\, U_a \quad , \tag{9}$$

$$\sigma_c^2 = 0.60 \times 10^{-3}\, U_a \quad , \tag{10}$$

where U_a is in meters per second and presumably measured at 15 feet above sea level. Once again σ^2 depends linearly on U_a. The difference between these estimates and those of Cox and Munk ((40)-(42) of Sec. 12.5) or those of Duntley ((18)-(21) of Sec. 12.5) is moderate, involving factors of 3 to 6, considering that only one wind speed was studied by SWOP.

In view of these findings, the stereo method of determining energy spectra seems on the whole marginally promising and certainly deserves to be further studied to see if it it feasible to increase the *resolving power* of the stereo pairs and to place more of the burden of the routine calculations on modern general-purpose computers with the goal in mind of a fully automated spectrum program. For on the one hand oceanographers will require as many accurate energy spectra gathered under as many diverse conditions as possible in the near future in order to evolve a comprehensive transport theory of the time dependent energy spectrum E(**k**,t); and the radiative transferists on the other hand will require still greater resolution of the capillary component of the energy spectrum, for the purpose of predicting radiant flux activity in natural waters, as affected by the air-water surface. Whether more comes of the stereo approach to wave energy spectra or not, the stereo wave observation project described above will stand as one of the more imaginative and prodigious projects of modern day optical oceanography.

Wave Spectra by Floating-Buoy Motion

The second of the two methods of determining wave spectra rests on the fact that, to a first approximation, the locus in space a small floating object on the air-water surface executes an orbital motion very nearly that of the packets of fluid at the surface (see observations following (63) of Sec. 12.3). If the object is small, light, and flat, not only will it take up the orbital motion of the surface water but also the orientations of the surface. If the flat floating object is a buoy which contains a recording accelerometer, then the twice-integrated acceleration vector will give ζ as a function of x,y and, especially, as a function of time t (cf. (7), (8) of Sec. 12.3). A pair of gyroscopes inside the floating buoy can give $\partial\zeta/\partial x$ and $\partial\zeta/\partial y$ as functions of time, provided the buoy is kept oriented by a sea anchor as depicted in Fig. 12.45. Hence the basic ingredients for a first order statistical description of the dynamic air-water surface would be available by this means.

The preceding scheme for recording ζ, $\partial\zeta/\partial x$, and $\partial\zeta/\partial y$ was used by Longuet-Higgins, Cartwright, and Smith [169] to obtain a working estimate of the energy spectrum $F(\sigma,\phi)$ (cf. (107) of Sec. 12.4) in some experiments in 1955 at the National Institution of Oceanography, England. The method was originally suggested by N. F. Barber [9] and was developed by Longuett-Higgins [163]. We shall now give a résumé of the method, as developed in [169].

The preceding description forms the physical part of the floating buoy method. It yet remains to translate the ζ , $\partial\zeta/\partial x$, and $\partial\zeta/\partial y$ data into a mathematical expression for $F(\sigma,\phi)$. The desired end product is a five term *finite* Fourier series expansion of $F(\sigma,\phi)$ defined by writing:

$$\text{"}F_1(\sigma,\phi)\text{"} \quad \text{for} \quad \frac{1}{2}a_0 + (a_1 \cos\phi + b_1 \sin\phi) + (a_2 \cos 2\phi + b_2 \sin 2\phi) \qquad (11)$$

where $F_1(\sigma,\phi)$ is the finite approximant to $F(\sigma,\phi)$, and where a_0, a_1, b_1, a_2, and b_2 are the required coefficients depending on the temporal frequency σ. It was found that the first five coefficients of the Fourier expansion of $F(\sigma,\phi)$ were adequate

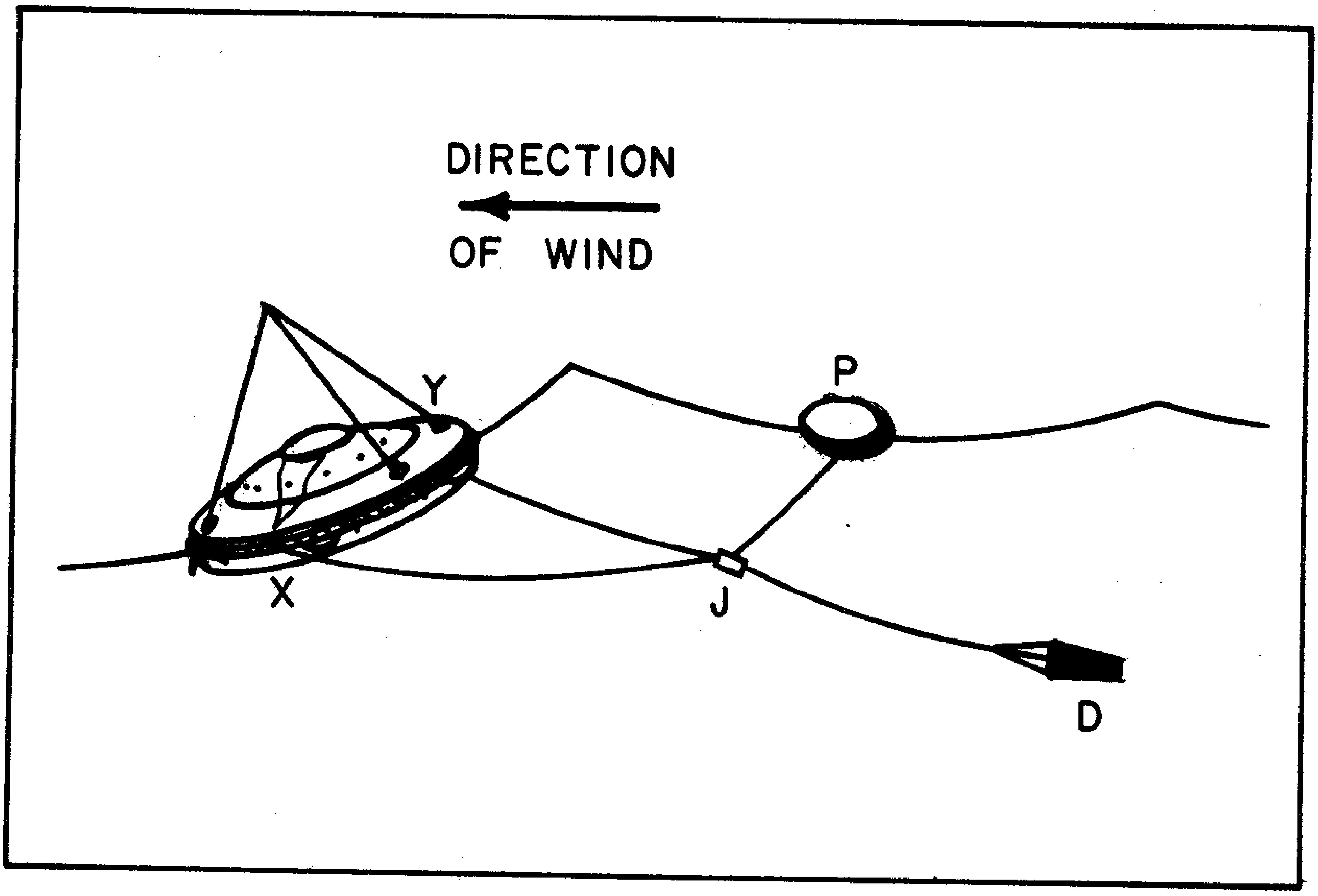

FIG. 12.45 Illustrating the floating buoy which carries recording linear and angular accelerometers to yield gravity wave-slope and wave-elevation data for use in determining the directional spectrum of the dynamic air-water surrace. A drogue bucket D and float arrangement of a pontoon P and line junction J keep the x and y axes of the float aligned parallel and perpendicular to the wind direction, respectively.

for the experiment under discussion. However, it is possible to obtain more terms of the Fourier expansion if the higher derivatives of ζ could be measured. A note was made in [169] to the effect that such a program was in progress.

Now, in order to obtain the five coefficients a_n and b_n, recall from (3), (4), and (7) of Sec. 12.4 that, on setting $p = \pi$, $a = 0$, we have in general:

$$a_n + i\, b_n = \frac{1}{\pi} \int_0^{2\pi} F(\sigma,\phi)\, e^{-in\phi}\, d\phi \quad . \qquad (12)$$

That is, the a_n and b_n are integrals of products of cosines or sines with $F(\sigma,\phi)$. Our studies of the moments m_{pq} in (116)-(119) of Sec. 12.4 suggest that the a_n and b_n are therefore closely related to the various moments m_{pq} when the spectrum $F(\sigma,\phi)$ (rather than $S(k,\phi)$) is used (cf. (88) of Sec. 12.4). The first few of these moments use only ζ and $\partial\zeta/\partial x$, $\partial\zeta/\partial y$. To see the exact connections, we start with (71) of Sec. 12.4 (with $\varepsilon = 0$) for a continuous spectrum:

$$\begin{aligned}\zeta(\mathbf{x},t) &= \mathcal{R}\int_{E_2} e^{i(\mathbf{k}\cdot\mathbf{x}-\sigma t)}\, dA(\mathbf{k}) \\ &= \int_{E_2} \mathcal{a}(\mathbf{k}) \cos\,(\mathbf{k}\cdot\mathbf{x}-\sigma t)\, dV(\mathbf{k}) \\ &= \int_{E_2} \mathcal{a}(\mathbf{k}) \cos\left[\frac{\sigma^2}{g}\,(x\cos\phi + y\sin\phi) - \sigma t\right] d\sigma\, d\phi \end{aligned} \tag{13}$$

where $k = \sigma^2/g$, $\mathbf{k} = (u(\sigma,\phi),\ v(\sigma,\phi))$, and where we have used the transformations following (107) of Sec. 12.4. From (13), by differentiation:

$$\frac{\partial\zeta(\mathbf{x},t)}{\partial x} = \mathcal{R}\int_{E_2} i\,k\cos\phi\; e^{i(\mathbf{k}\cdot\mathbf{x}-\sigma t)}\, dA(\mathbf{k}) \tag{14}$$

and once again from (13):

$$\frac{\partial\zeta(\mathbf{x},t)}{\partial y} = \mathcal{R}\int_{E_2} i\,k\sin\phi\; e^{i(\mathbf{k}\cdot\mathbf{x}-\sigma t)}\, dA(\mathbf{k}) \quad . \tag{15}$$

With these preliminaries established we now continue with the main part of the description of how the coefficients a_0, a_1, b_1, a_2, b_2 are obtained in practice. The records of ζ, $\partial\zeta/\partial x$, $\partial\zeta/\partial y$ are time records obtained over a period of time at essentially one point in space. Therefore the requisite statistical information contained in their records is unlocked by performing appropriate autocorrelation and cross correlation operations on these functions. Thus, for brevity, let us write "ξ_1", "ξ_2", "ξ_3" for ζ, $\partial\zeta/\partial x$, and $\partial\zeta/\partial y$, respectively. Then writing:

$$\text{"}\phi_{ij}(t)\text{"} \quad \text{for} \quad \lim_{T\to\infty} \frac{1}{2T}\int_{-T}^{T} \xi_i(t+\tau)\ \xi_j(\tau)\ d\tau \tag{16}$$

we can obtain the spectrum of $\phi_{ij}(t)$, $i,j = 1, 2, 3$, in the usual manner by writing:

$$\text{"}D_{ij}(\sigma)\text{"} \quad \text{for} \quad \lim_{T\to\infty} \int_{-T}^{T} \phi_{ij}(t)\, e^{-i\sigma t}\, dt \quad . \tag{17}$$

Whenever $i = j$ (i.e., when we take the autocorrelation function of ξ_i) $D_{ij}(\sigma)$ is real, since ϕ_{ij} is an even function. Thus if we explicitly represent $D_{ij}(\sigma)$ as:

$$D_{ij}(\sigma) = C_{ij}(\sigma) + i\, Q_{ij}(\sigma) \quad , \tag{18}$$

then $Q_{ii}(\sigma) = 0$. The functions C_{ij} for $i \neq j$ are called the *co-spectra* of ξ_i and ξ_j; and Q_{ij} are called the *quadrature spectra* of ξ_i and ξ_j. It is now easy to show, using the representations (13)-(15) of ξ_1, ξ_2, ξ_3 in (17), that:

$$C_{11}(\sigma) = \int_0^{2\pi} F(\sigma,\phi)\, d\phi \tag{19}$$

$$C_{22}(\sigma) = \int_0^{2\pi} k^2 \cos^2\phi\, F(\sigma,\phi)\, d\phi \tag{20}$$

$$C_{33}(\sigma) = \int_0^{2\pi} k^2 \sin^2\phi\, F(\sigma,\phi)\, d\phi \tag{21}$$

$$C_{23}(\sigma) = \int_0^{2\pi} k^2 \sin\phi \cos\phi\, F(\sigma,\phi)\, d\phi \tag{22}$$

$$Q_{12}(\sigma) = \int_0^{2\pi} k \cos\phi\, F(\sigma,\phi)\, d\phi \tag{23}$$

$$Q_{13}(\phi) = \int_0^{2\pi} k \sin\phi\, F(\sigma,\phi)\, d\phi \quad . \tag{24}$$

These relations give the requisite working link between the computables C_{ij}, Q_{ij} and the desirables a_0, a_1, b_1, a_2, b_2; for by placing $F_1(\sigma,\phi)$ as given by (11), into (12), and sorting out the results using (19)-(24) (for $F_1(\sigma,\phi)$) and by the uniqueness of the desired Fourier coefficients we eventually arrive at:

$$a_0 = \frac{1}{\pi} C_{11} \tag{25}$$

$$a_1 = \frac{1}{\pi k} Q_{12} \quad , \quad b_1 = \frac{1}{\pi k} Q_{13} \tag{26}$$

$$a_2 = \frac{1}{\pi k^2} (C_{22} - C_{33}) \quad , \quad b_2 = \frac{2}{\pi k^2} C_{23} \quad . \tag{27}$$

One final point in the computations of the coefficients in (11) is to be noted. The spectrum $F(\sigma,\phi)$ is never negative, by definition. It is possible, however, for its finite approximant $F_1(\sigma,\phi)$ to be negative. Indeed, since

$$F_1(\sigma,\phi) = \frac{1}{2\pi} \int_0^{2\pi} F(\sigma,\phi') \, W_1(\phi'-\phi) \, d\phi' \quad , \qquad (28)$$

where we have written

$$\text{"}W_1(\phi'-\phi)\text{"} \quad \text{for} \quad 1 + 2\cos(\phi'-\phi) + 2\cos 2(\phi'-\phi) \quad ; \qquad (29)$$

it is clear that W_1 and hence F_1 can be negative for some ϕ. To avoid negative values of $F_1(\sigma,\phi)$, a new approximant of $F(\sigma,\phi)$ is defined by writing:

$$\text{"}F_3(\sigma,\phi)\text{"} \quad \text{for} \quad \frac{1}{2} a_0 + \frac{2}{3}(a_1 \cos\phi + b_1 \sin\phi) + \frac{1}{6}(a_2 \cos 2\phi + b_2 \sin 2\phi) . \qquad (30)$$

The theory leading to the coefficients a_0, a_1, b_1, a_2, b_2 in (30) is still that summarized in (25)-(27). Once these five numbers have been found, $F_3(\sigma,\phi)$ is constructed as shown, the result being a nonnegative function of ϕ and representable as:

$$F_3(\sigma,\phi) = \frac{1}{2\pi} \int_0^{2\pi} F(\sigma,\phi') \, W_3(\phi'-\phi) \, d\phi' \qquad (31)$$

where we write:

$$\text{"}W_3(\phi'-\phi)\text{"} \quad \text{for} \quad 1 + \frac{4}{3}\cos(\phi'-\phi) + \frac{1}{3}\cos 2(\phi'-\phi) \quad . \qquad (32)$$

It is $F_3(\sigma,\phi)$ (and not $F_1(\sigma,\phi)$) that is the chosen finite approximant to $F(\sigma,\phi)$ in [169]. This completes the exposition of one form of theory of obtaining the energy spectrum $F(\sigma,\phi)$ from floating-buoy motions.

An example of the results of the study [169] will now be given. Figure 12.46 shows histograms of the surface elevation ζ of the sea, and the *angles* corresponding to the slopes $\partial\zeta/\partial x$, $\partial\zeta/\partial y$. The gaussian forms of the distributions are evident, at least on a visual level, attesting to the linearity of the waves (i.e., the slopes were still small enough so that $\alpha \cong \tan\alpha$, for either pitch or roll angle α). The recorded results are for an anemometer wind speed of 23 knots, with a fetch of over 300 miles. The root mean square elevation was 2.6 feet.

Figure 12.47 gives a plot of computed T_0 (= $C_{11}(\sigma)$) for the same recorded run (number 5) as that in Fig. 12.46. The dashed line is the form of Phillips' theoretical limiting spectrum for an equilibrium sea (cf. [198]).

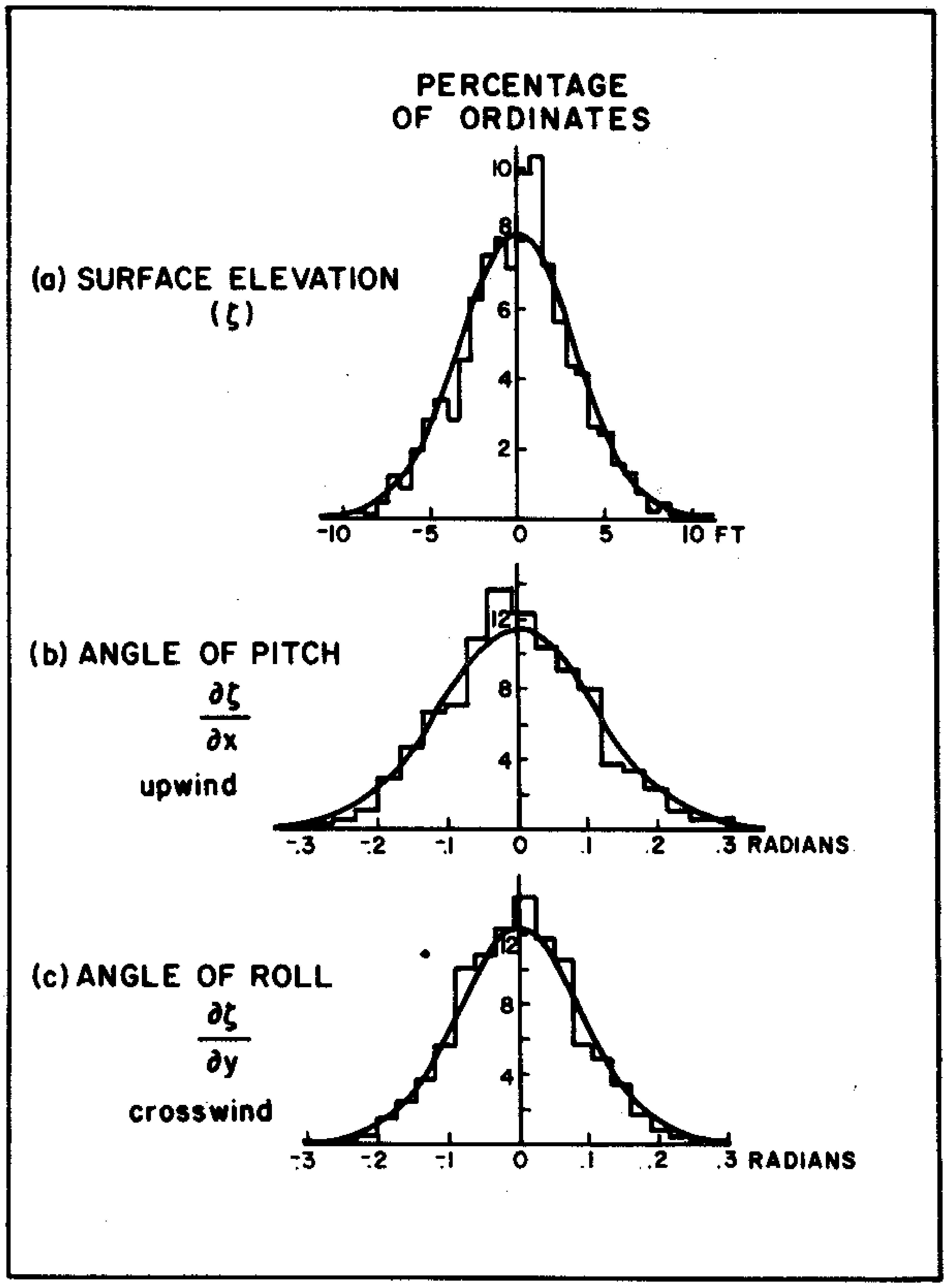

FIG. 12.46 Statistical distribution of vertical and angular displacements of the recording buoy of Fig. 12.45. (For an anemometer wind speed of 23 knots with a fetch of over 300 miles.)

Figure 12.48 depicts F (σ,ϕ) as computed from record No. 5. Hence Figs. 12.46-12.48 give a complete spectral documentation and geometric documentation of the sea surface under the given conditions, which may be used to predict the average reflectance and transmittance of the air-water surface, under the same conditions, using the theory of Sec. 12.11.

The co-spectra and quadrature spectra played essential roles in the present method. For a general study of the empirical estimations of such spectra, see [99].

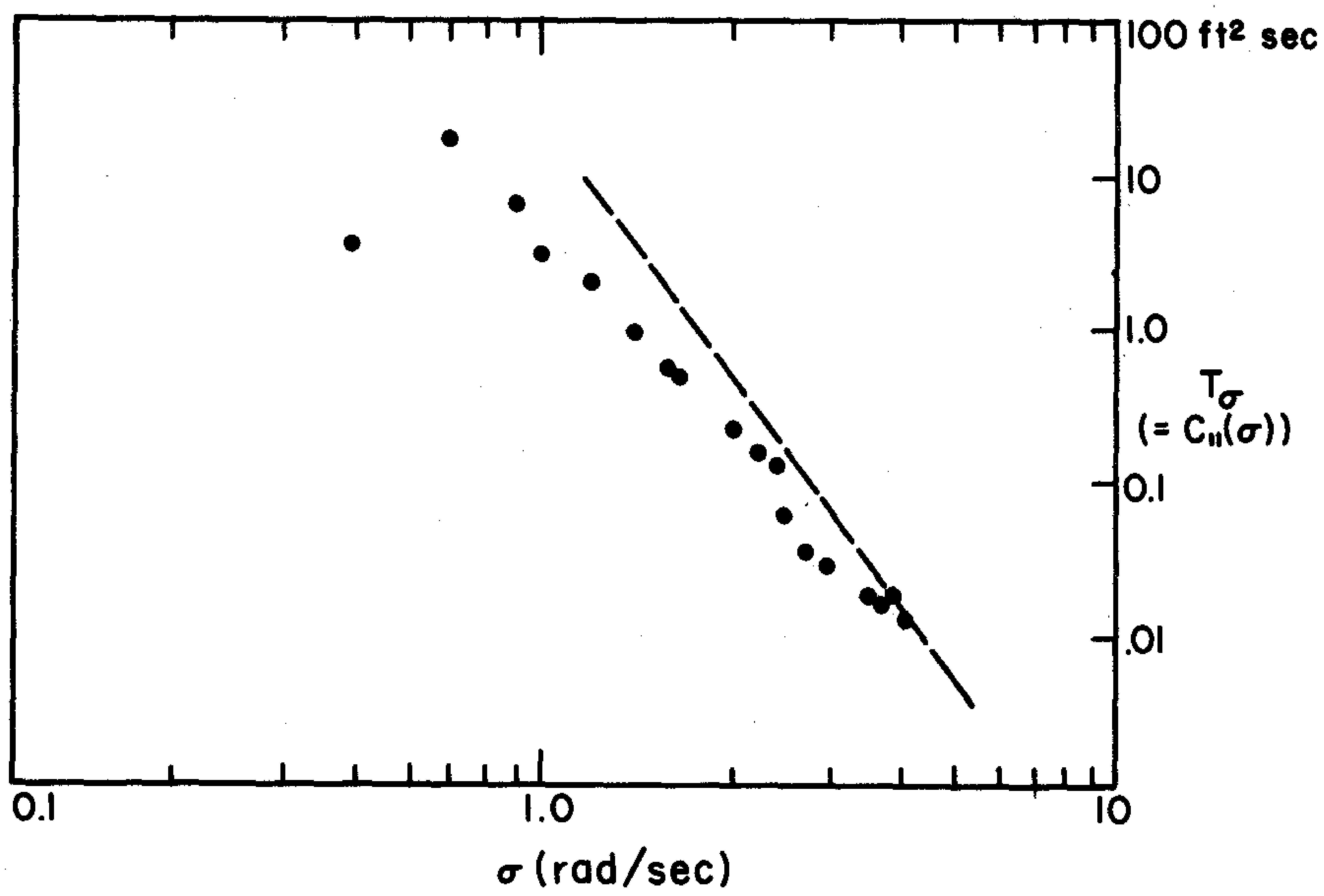

FIG. 12.47 A plot of T_σ vs. σ for the same data run of Fig. 12.46.

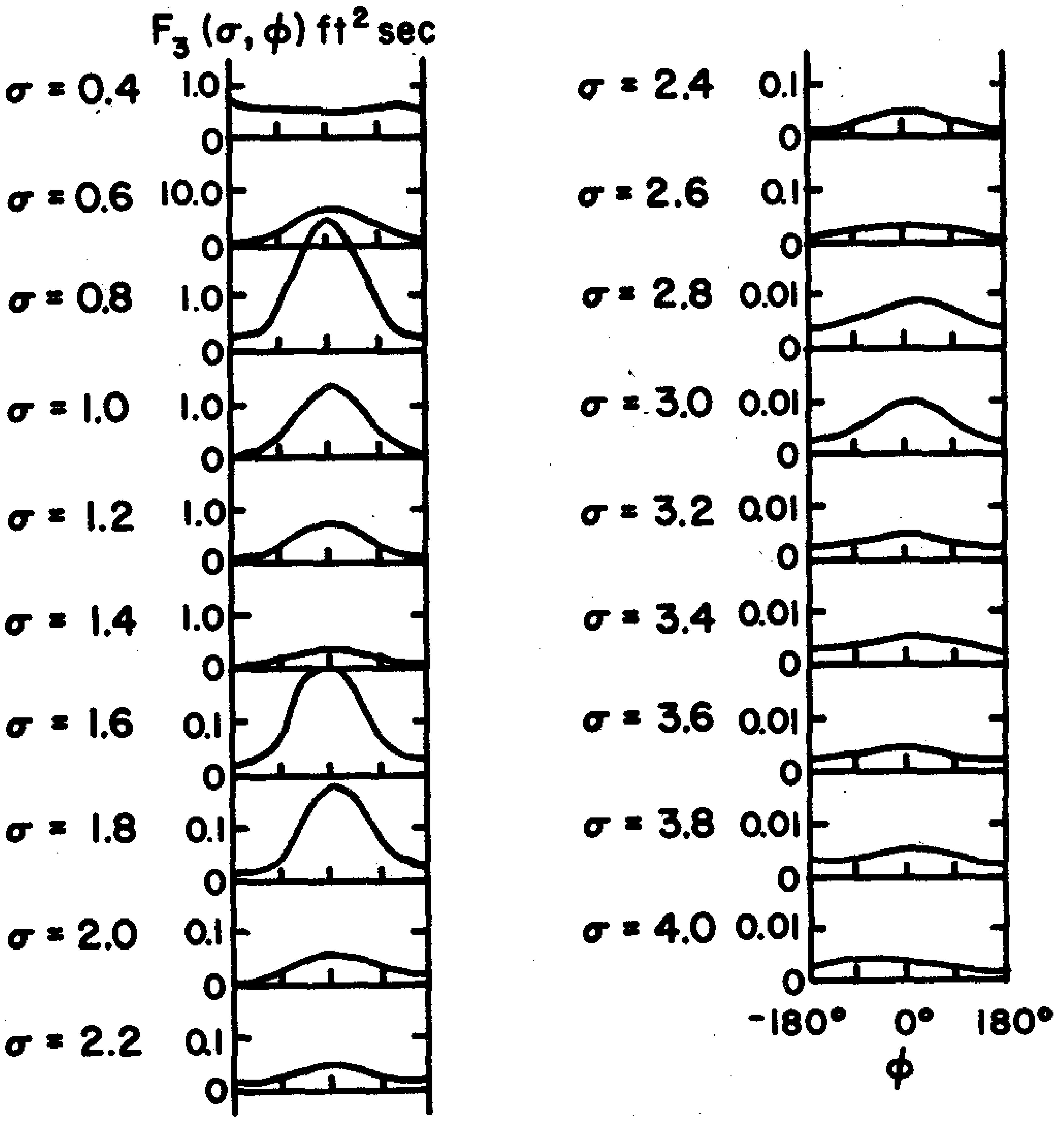

FIG. 12.48 Directional spectrum $F_3(\sigma, \phi)$ for the same data run of Fig. 12.46. Figures 12.45-12.48 are adapted from a study by Longuet-Higgins, Cartwright, and Smith (Record No. 5).

Wave Spectra from Submarine Echo Recordings

We close our survey of some experimental means of determining the energy spectrum of the dynamic air-water surface by noting that submarines have been used to good effect as submerged hovering platforms on which echo sounders have been mounted, directed upward at the sea surface, and the relative wave heights measured by continually dividing the echo travel time by the speed of sound in water. For example, the submarine U.S.S. *Red Fin* in the fall of 1960, 200 miles east of Cape Hatteras, North Carolina, obtained for the U.S. Hydrographic Office, records of echo soundings of the surface at keel depths of 80 to 100 feet, with the submarine drifting at about 1 knot and sending a sonic beam of 3° spread up toward the surface. Further details are given by de Leonibus [64]. Since only one echo sounder was used, the data are equivalent to taking wave height readings from an anchored pole in the sea, so that only T_σ or T_τ, or any of the other one-dimensional spectra can be determined. A sample of the data in the form of the temporal frequency spectrum T_σ (cf. (110) of Sec. 12.4) is given in Fig. 12.49.

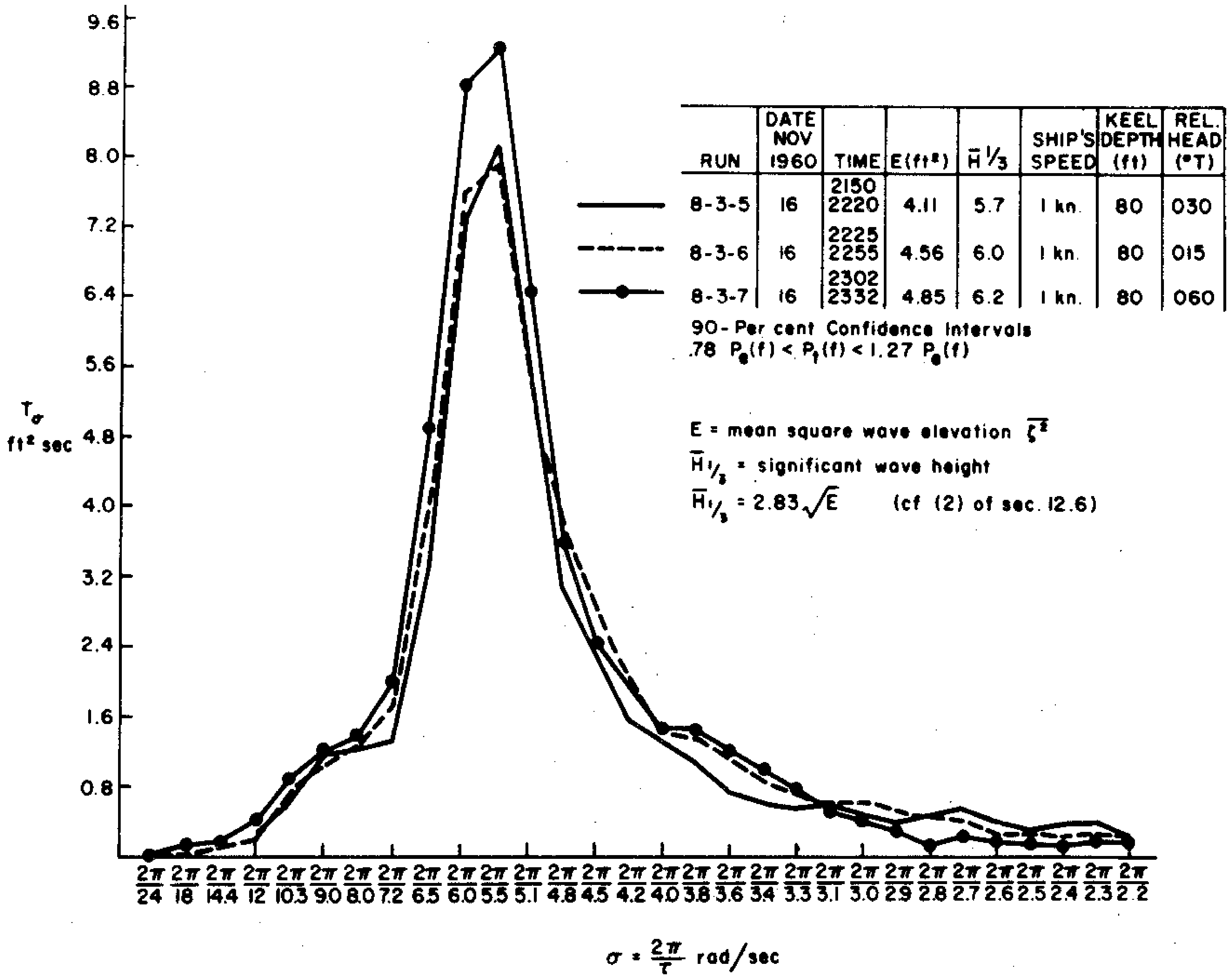

	RUN	DATE NOV 1960	TIME	E(ft²)	$\bar{H}_{1/3}$	SHIP'S SPEED	KEEL DEPTH (ft)	REL. HEAD (°T)
———	8-3-5	16	2150 2220	4.11	5.7	1 kn.	80	030
- - - -	8-3-6	16	2225 2255	4.56	6.0	1 kn.	80	015
—●—	8-3-7	16	2302 2332	4.85	6.2	1 kn.	80	060

90-Per cent Confidence Intervals
$.78\ P_e(f) < P_t(f) < 1.27\ P_e(f)$

E = mean square wave elevation $\overline{\zeta^2}$
$\bar{H}_{1/3}$ = significant wave height
$\bar{H}_{1/3} = 2.83\sqrt{E}$ (cf (2) of sec. 12.6)

FIG. 12.49 Wave energy spectrum T_σ as determined by de Leonibus using sonar equipment mounted on a submerged hovering submarine.

<< Table of Contents << Title Page >> Next Page >>